IEEE Access
Multidisciplinary | Rapid Review | Open Access Journal

Received April 27, 2020, accepted May 7, 2020, date of publication May 12, 2020, date of current version May 22, 2020.

Digital Object Identifier 10.1109/ACCESS.2020.2993985

Fixed Point Implementation of Grid Tied Inverter in Digital Signal Processing Controller

SHUVANGKAR SHUVO[1], (Member, IEEE), EKLAS HOSSAIN[2], (Senior Member, IEEE), AND ZIAUR RAHMAN KHAN[1]

[1]Department of Electrical and Electronic Engineering, Bangladesh University of Engineering and Technology, Dhaka 1205, Bangladesh
[2]Oregon Renewable Energy Center (OREC), Department of Electrical Engineering and Renewable Energy, Oregon Institute of Technology, Klamath Falls, OR 97601, USA

Corresponding author: Shuvangkar Shuvo (sshuvo93@gmail.com)

ABSTRACT Power inverters are one of the devices of great importance used in power grids to convert DC to AC, especially for grids with attached solar panels or wind turbines. The world is getting warmer due to coal- and oil-based power generation. So human existence is threatened due to the increased amount of carbon-dioxide in the air. As a result, integration of renewable energy sources (RESs) with the grid became mandatory. So, the demand of grid-connected inverters is increasing as more RESs are connecting with the grid; this necessitates developing a low-cost grid connected inverter system. This paper presents a comprehensive study and hardware implementation of a grid tied inverter. In this research, we have demonstrated a cost-efficient grid tied inverter design using low cost DSP controller applying fixed point arithmetic. The fixed-point arithmetic and Digital Signal Processing (DSP) implementation results in superior performance over conventional methods of calculation. This paper also proposes a hardware model of such a bi-directional grid tied inverter. A current controlled Voltage Source Inverter(VSI) is used in the paper and a PI controller is suggested for current error compensation. To generate gating pulse for appropriate voltage, Space Vector Pulse Width Modulation (SVPWM) technique is employed. Synchronous Reference Frame Phase Locked Loop (SRF-PLL) is chosen for performing grid synchronization. The feasibility of the hardware model is verified by performing simulations on Simulink.

INDEX TERMS Inverter, grid-tied inverter, PWM-Rectifier, microgrid, renewable energy grid integration, energy storage systems, SVPWM, PI controller, synchronous reference frame PLL (SRF-PLL).

I. INTRODUCTION

Inverters are the most salient part of a grid for integrating renewable energy sources (RESs). They play a crucial role in DC to AC conversion. Electrical energy is usually stored as DC in energy storage systems (ESSs). To recover the stored energy, it is necessary to convert it into AC to feed to the utility grid for consumption. A grid tied inverter differs from a conventional inverter to a few extents. Grid tied inverters continuously maintain synchronization with the grid as well as control real and reactive power. Two systems are said to be synchronized when the voltages are in phase with each other and the frequency is the same. So, when inverters are synchronized to the grid, it means that the inverter output voltage and the grid voltage should have a phase difference of 0° and the two voltages should have the same frequency.

The associate editor coordinating the review of this manuscript and approving it for publication was Ramazan Bayindir.

Solar panels or wind turbines used as sources in grids produce DC voltage which needs to be converted to AC voltage for supplying to utility. For grids focused on photovoltaic (PV), several grid-connected inverter models have been proposed. A soft switched inverter consisting of reduced component size and power switches are demonstrated in [1]. An improved cascade-type control scheme is proposed in [2] to achieve fast transient response and low total harmonic distortion (THD). It was noticed in [3] that parasitic capacitors between PV panels and the earth causes leakage current in cascaded-multilevel inverters. To mitigate such problems, filter-based solutions have garnered popularity. A single phase LLCL filter based Aalborg inverter [4] can vary its input DC value for a wide range and save the total inductance for the conventional voltage source inverter (VSI). Transformerless inverters have recently paved their way into the field because of their light weight and low cost. A modular buck-boost transformer less inverter is represented in [5] for low voltage solar panels. Current control mode is used

to control the inverter for the purpose of shaping current to adjust power delivery. A modified multilevel cascaded H-Bridge inverter has been designed and implemented [6] for PV systems. Another compact three phase multilevel inverter has been designed in [7] using a single DC source in each phase for generating multiple level output voltages. This is suitable for low and medium voltage applications, including grid integration of renewables or energy storage systems.

The contributions of this paper are to manifest a cost-efficient grid-tied inverter using fixed point arithmetic and digital signal processing and to implement a small-scale hardware prototype grid tied inverter. A current controlled VSI is used in the paper and a PI controller is suggested for current error compensation. To generate gating pulse for appropriate voltage, Space Vector Pulse Width Modulation (SVPWM) technique is employed. Synchronous Reference Frame Phase Locked Loop (SRF-PLL) is chosen for performing grid synchronization. The feasibility of the hardware model is verified by performing simulations on Simulink. The schematic diagram of the proposed system is illustrated in Figure 1.

Similar works have been performed by many researchers as numerous attempts have been made to improve inverters for grid connection for renewable energy penetration. For instance, in 2012, Abdalrahman et al have demonstrated a comprehensive simulation and implementation of a three-phase grid-connected inverter using the PSIM simulation package [8]. In 2014, Al-Durra et al have presented a three-phase grid tied DC/AC inverter with active and reactive power (VAR) control for medium size renewable and distributed DC energy sources [9]. In 2018, Sevilmi et al have simulated an experimental three-phase grid tied inverter controlled by SVPWM method for RESs [10]. A compact three phase multilevel inverter for low and medium power PV systems has been explored in [7]. Inverters are a relatively new subject in the field of power electronics, and are under continual development. This study is a humble attempt at enriching that branch with an updated and improved technology.

The rest of the paper is organized as follows: Section II presents the modelling of the proposed system using relevant equations. Section III represents the real and reactive power control methods of the inverter and involves derivation of the different transformation and control techniques for grid tied inverter with simulation results. Section IV explains the grid synchronizing process using SRF-PLL system and the generation of the gating pulses using SVPWM method. Section V discusses the fixed-point arithmetic and how it is used in the proposed system to calculate the PLL angle. Section VI analyses the experimental results and demonstrates the integrated hardware implementation. Section VII draws out the conclusion to the paper.

II. SYSTEM MODELLING

A DC motor torque equation is governed by

$$I_f I_a = k I_d I_q \tag{1}$$

Here I_f and I_a are field current and armature current respectively. So, the torque of a DC motor can be controlled precisely using a standard PI controller, which works robustly on DC quantities of I_f and I_a. However, a PI controller inherently cannot maintain zero steady state error for sinusoidal reference. The integral action removes the error if reference value is constant in steady state. So, to control the sinusoidal output current, it is convenient to transform the sinusoidal or alternating current or voltage into DC quantities through dq transform. Thus, the model in dq frame is derived from three phase a-b-c frame. The conversion process comprises of two steps: firstly, from abc frame to $\alpha\beta$ frame by means of Clarke Transformation, and then from $\alpha\beta$ frame to the dq frame using Park Transformation.

The basic circuit for a three-phase grid tied inverter is depicted in Figure 2. The sinusoidal three phase output voltage of inverter is as follows

$$v_{ia} = A sin\,(\omega t) \tag{2}$$

$$v_{ib} = A sin\left(\omega t - \frac{2\pi}{3}\right) \tag{3}$$

$$v_{ic} = A sin\left(\omega t + \frac{2\pi}{3}\right) \tag{4}$$

Here, A is the amplitude of voltage, ω is the angular frequency and v_{ia}, v_{ib}, v_{ic} are three phase inverter side voltages. The generic equation for a single phase is derived as

$$v_i = v_L + v_R + v_g \tag{5}$$

$$v_i = L\frac{di}{dt} + iR + v_g \tag{6}$$

$$v_g = v_i - L\frac{di}{dt} - iR \tag{7}$$

The equation matrix for three phase stationary frame is

$$\begin{bmatrix} v_{ga} \\ v_{gb} \\ v_{gc} \end{bmatrix} = \begin{bmatrix} v_{ia} - L\dfrac{di_a}{dt} - Ri_a \\ v_{ib} - L\dfrac{di_b}{dt} - Ri_b \\ v_{ic} - L\dfrac{di_c}{dt} - Ri_c \end{bmatrix} \tag{8}$$

The equation for the transformation of three phase stationary (abc) to two phase stationary ($\alpha\beta$) would be

$$\begin{bmatrix} v_{g\alpha} \\ v_{g\beta} \end{bmatrix} = \frac{2}{3}\begin{bmatrix} 1 & -\frac{1}{2} & -\frac{1}{2} \\ 0 & \frac{\sqrt{3}}{2} & -\frac{\sqrt{3}}{2} \end{bmatrix}\begin{bmatrix} v_{ga} \\ v_{gb} \\ v_{gc} \end{bmatrix} \tag{9}$$

$$= \frac{2}{3}\begin{bmatrix} 1 & -\frac{1}{2} & -\frac{1}{2} \\ 0 & \frac{\sqrt{3}}{2} & -\frac{\sqrt{3}}{2} \end{bmatrix}\begin{bmatrix} v_{ia} - L\dfrac{di_a}{dt} - Ri_a \\ v_{ib} - L\dfrac{di_b}{dt} - Ri_b \\ v_{ic} - L\dfrac{di_c}{dt} - Ri_c \end{bmatrix} \tag{10}$$

$$\begin{bmatrix} v_{g\alpha} \\ v_{g\beta} \end{bmatrix} = \begin{bmatrix} v_{i\alpha} - L\dfrac{di_\alpha}{dt} - Ri_\alpha \\ v_{i\beta} - L\dfrac{di_\beta}{dt} - Ri_\beta \end{bmatrix} \tag{11}$$

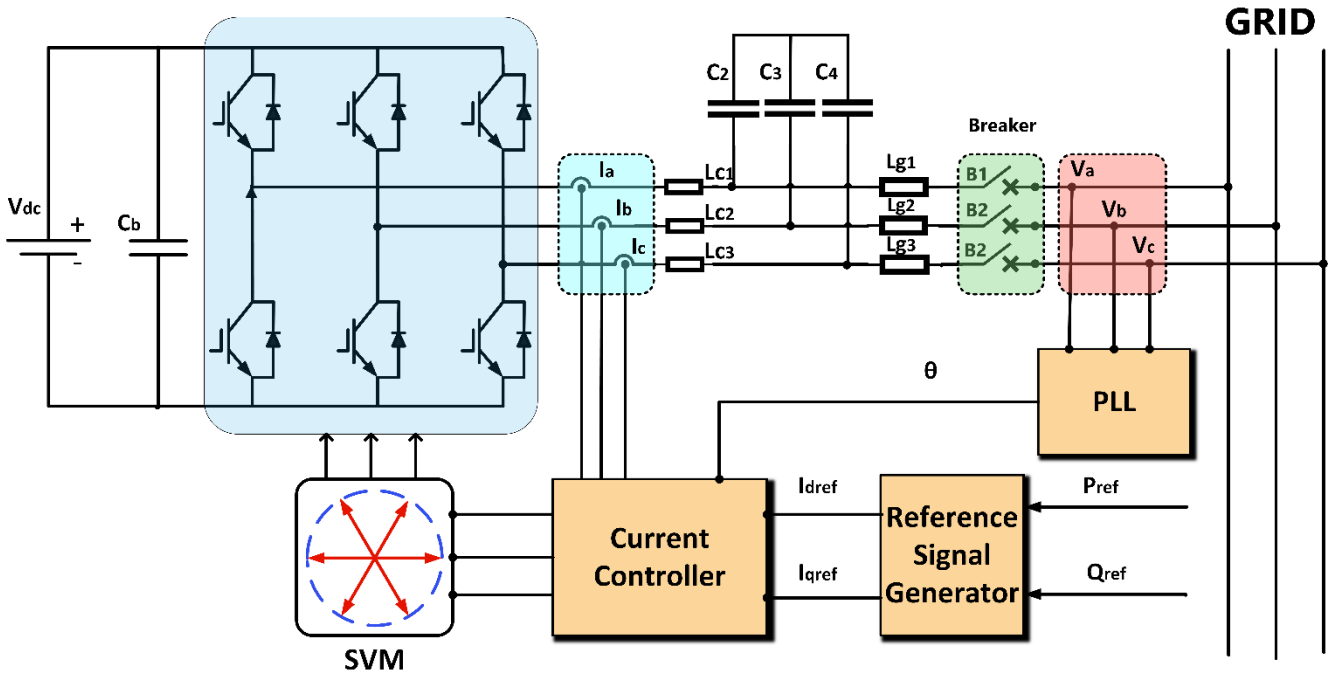

FIGURE 1. Schematic diagram of the whole proposed system of the three-phase grid tied DC/AC inverter, comprising of a three-phase inverter, a current control system, gating pulse generator for the inverter switches and a grid synchronizing system.

Now, for converting from the $\alpha\beta$ frame to the synchronous d-q frame

$$\begin{bmatrix} v_{gd} \\ v_{gq} \end{bmatrix} = \begin{bmatrix} cos\omega t & sin\omega t \\ -sin\omega t & cos\omega t \end{bmatrix} \begin{bmatrix} v_{g\alpha} \\ v_{g\beta} \end{bmatrix} \tag{12}$$

$$\begin{bmatrix} v_{gd} \\ v_{gq} \end{bmatrix} = \begin{bmatrix} cos\omega t & sin\omega t \\ -sin\omega t & cos\omega t \end{bmatrix} \begin{bmatrix} v_{i\alpha} - L\dfrac{di_\alpha}{dt} - Ri_\alpha \\ v_{i\beta} - L\dfrac{di_\beta}{dt} - Ri_\beta \end{bmatrix} \tag{13}$$

$$\begin{bmatrix} v_{gd} \\ v_{gq} \end{bmatrix} = \begin{bmatrix} v_{id} \\ v_{iq} \end{bmatrix} - R\begin{bmatrix} i_d \\ i_q \end{bmatrix} - L\begin{bmatrix} cos\omega t & sin\omega t \\ -sin\omega t & cos\omega t \end{bmatrix} \begin{bmatrix} \dfrac{di_\alpha}{dt} \\ \dfrac{di_\beta}{dt} \end{bmatrix} \tag{14}$$

Now,

$$\begin{bmatrix} cos\omega t & sin\omega t \\ -sin\omega t & cos\omega t \end{bmatrix} \begin{bmatrix} \dfrac{di_\alpha}{dt} \\ \dfrac{di_\beta}{dt} \end{bmatrix} = \frac{d}{dt}\begin{bmatrix} i_d \\ i_q \end{bmatrix} + \omega \begin{bmatrix} -i_q \\ i_d \end{bmatrix} \tag{15}$$

So, the electrical dynamics of inverter in d-q synchronous frame is derived as

$$\begin{bmatrix} v_{gd} \\ v_{gq} \end{bmatrix} = \begin{bmatrix} v_{id} \\ v_{iq} \end{bmatrix} - R\begin{bmatrix} i_d \\ i_q \end{bmatrix} - L\frac{d}{dt}\begin{bmatrix} i_d \\ i_q \end{bmatrix} - \omega L \begin{bmatrix} -i_q \\ i_d \end{bmatrix} \tag{16}$$

$$\begin{bmatrix} v_{id} \\ v_{iq} \end{bmatrix} = \begin{bmatrix} v_{gd} \\ v_{gq} \end{bmatrix} + L\frac{d}{dt}\begin{bmatrix} i_d \\ i_q \end{bmatrix} + \omega L \begin{bmatrix} -i_q \\ i_d \end{bmatrix} + R\begin{bmatrix} i_d \\ i_q \end{bmatrix} \tag{17}$$

The resistance R can be practically neglected and the differential equation of synchronous frame becomes

$$\frac{d}{dt}\begin{bmatrix} i_d \\ i_q \end{bmatrix} = \frac{1}{L}\begin{bmatrix} v_{id} - v_{gd} \\ v_{iq} - v_{gq} \end{bmatrix} - \omega \begin{bmatrix} -i_q \\ i_d \end{bmatrix} \tag{18}$$

The equation describes that the dynamics of one axis current is dependent on the other axis current. This is analogous to the electric machine where direct axis flux produces quadrature axis back EMF. The control scheme is illustrated in Figure 3.

To control the currents $i_d and i_q$, a PI controller is proposed. Thus, the inverter input reference voltage would be

$$\begin{bmatrix} v_{id}^* \\ v_{iq}^* \end{bmatrix} = \begin{bmatrix} v_{gd} \\ v_{gq} \end{bmatrix} + \begin{bmatrix} (k_p + \dfrac{k_i}{s})(i_d^* - i_d) \\ (k_p + \dfrac{k_i}{s})(i_q^* - iq) \end{bmatrix} + \omega L \begin{bmatrix} -i_q \\ i_d \end{bmatrix} \tag{19}$$

Here, the asterisk $(*)$ sign indicates the reference variable.

III. REAL POWER AND REACTIVE POWER CONTROL

There are two control strategies for three phase Voltage Source Inverters (VSI): current control and voltage control. Voltage controlled VSI uses the phase difference between the inverter output voltage and grid voltage to control the power flow. Current-controlled VSI provides high-accuracy control of instantaneous current, protection from peak-current, overload mitigation, and superior dynamics [11]. In the past few years, many current control strategies have been developed. The major types of pulse width modulation (PWM) based current control strategies are linear and non-linear.

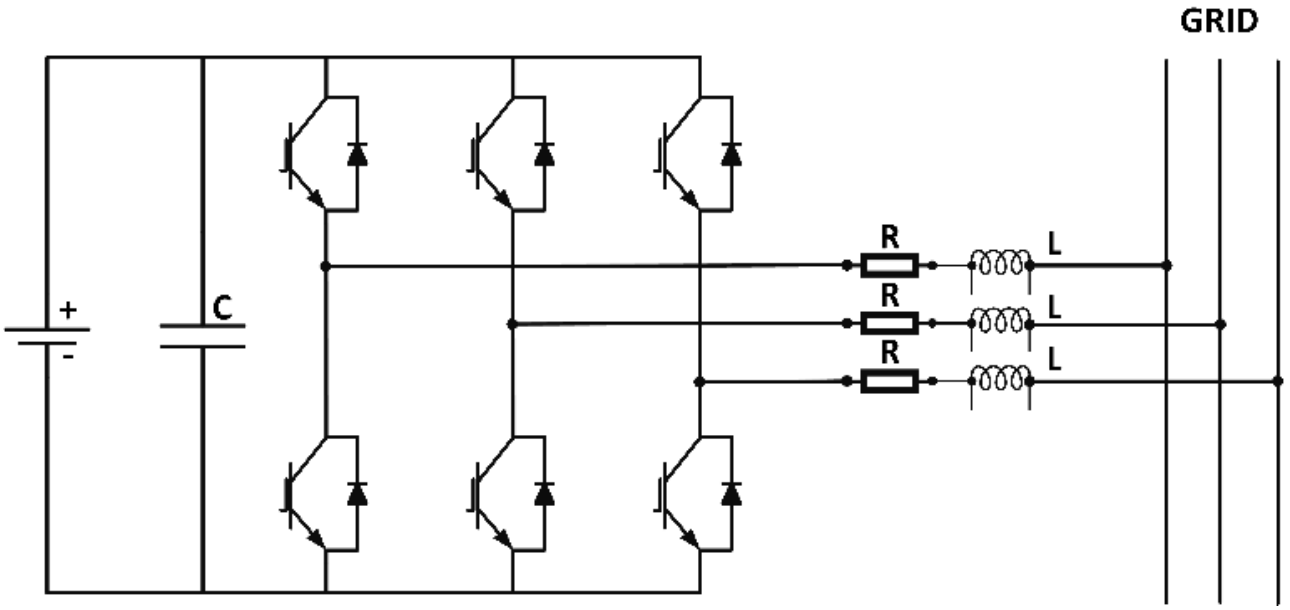

FIGURE 2. Circuit diagram of a three-phase grid tied inverter. The inverter consists of six switches paralleled by freewheeling diodes. A dc-link capacitor stores the voltage temporarily before transmitting it to the inverter. The inverter is connected to the AC grid by means of lines that are equivalent to RL branches.

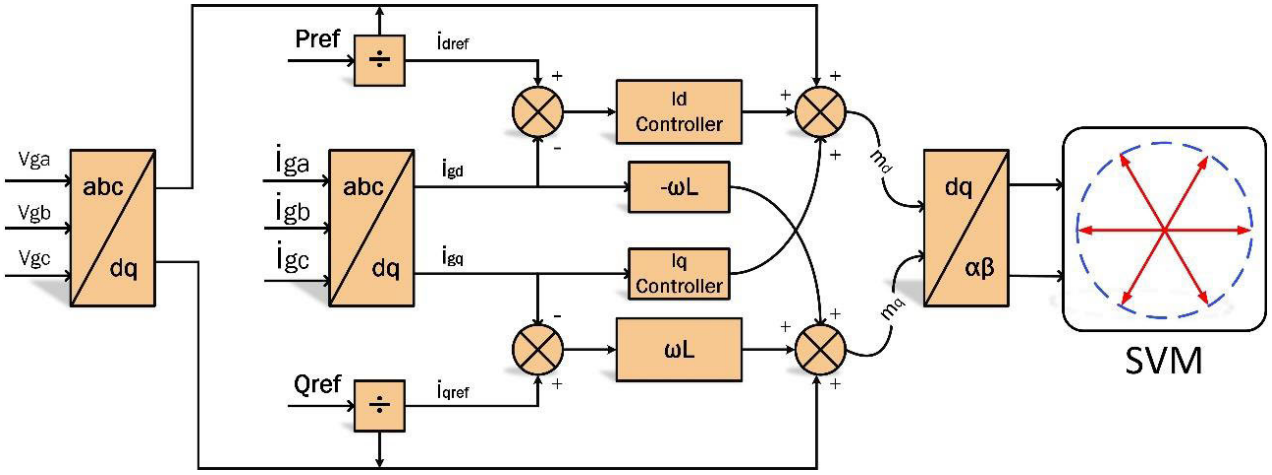

FIGURE 3. Block diagram of Control Schema derived from the mathematical model of grid tied inverter.

Linear control strategies include Proportional Integral (PI) Controller, Proportional Resonant (PR) Controller, Predictive Dead-beat Controller and Repetitive Controller. Non-linear control strategies include Hysteresis Controller, Delta modulation and On-line optimized controller.

Predictive controller has a very good steady-state performance and provides a good dynamic performance. However, its performance is sensitive to system parameters. The hysteresis controller has fast transient response, non-complex implementation and an inherent current protection. However, the hysteresis controller has some drawbacks such as variable switching frequency and high current ripples. These cause poor current quality and introduce difficulties in the output filter design [12], [13].

The main principle of current control is to force the controller current to follow the reference signal. In case of current control strategy, active and reactive components of the current injected into grid are controlled separately using PWM techniques. The proposed model of inverter operates in linear current control mode because the grid controls the operating voltage and frequency. The inverter has nothing to do with voltage and frequency as it is connected with infinite bus. The controller sets the current reference by which it controls real and reactive power as shown in Figure 3. A prominent advantage is that current control is less sensitive to distorted grid voltage and its response is faster. For these reasons, current control has advantages over voltage control methods. Thus, for grid connected application, current control is

TABLE 1. Comparison among the three main current controllers.

Parameter	Hysteresis Current Controller	Predictive Current Controller	Linear PI Current Controller
Steady State Response	High THD, high current ripple, and variable switching frequency	Low THD	Very low THD, even with high distorted grid
Sensitivity to system parameters	None	Sensitive to system parameters	None
Dynamic Response	Very fast	Very fast	Slightly inferior than others

recommended. The current controller for controlling current in the grid connected inverters are vastly classified according to Figure 4.

Table 1 summarizes the advantages and disadvantages of three principle current controllers: hysteresis current controller, predictive current controller and linear PI current controller. Based on these judgements, the linear PI control algorithm is found to be the best choice to implement the grid connected inverter [14], although PI controllers also have some problems, such as limited bandwidth, poor disturbance rejection and introduction of delay into the control loop [**?**].

The equations for calculation of current reference are deduced as follows. As all the calculations are in the d-q axis, thus the real and reactive power equations of inverter are respectively governed by

$$P_{dq} = \frac{3}{2}\left(V_d I_d + V_q I_q\right) \tag{20}$$

$$Q_{dq} = \frac{3}{2}\left(V_q I_d - V_d I_q\right) \tag{21}$$

Solving the equations, we can get the reference direct axis (I_d) and quadrature axis (I_q) current reference value

$$i_d^* = \frac{2}{3}\left(\frac{P_{dq}V_d - Q_{dq}V_q}{V_d^2 + V_q^2}\right) \tag{22}$$

$$i_q^* = \frac{2}{3}\left(\frac{P_{dq}V_q - Q_{dq}V_d}{V_d^2 + V_q^2}\right) \tag{23}$$

These reference currents represent i_{dref} and i_{qref} in Figure 3, which are fed into the PI Controller to push real and reactive power into the grid.

The PI current control offers an excellent steady-state response, low current ripple, constant switching frequency and well-defined harmonic content. Moreover, the controller is insensitive to system parameters since the algorithm does not need system models [15]. In this system, PI controllers are used to compensate the current vector components that are defined in synchronous reference frame. Because of coordinate transformations, i_d and i_q are DC components, and therefore reduce the error(s) between the reference current I_d^* (I_q^*) and the actual current I_d (I_q) to zero [12]. PI controller performs better in stationary systems as d-q components of current represent the AC parameters as dc quantities.

The equation of the PI controller is

$$u(t) = k_p e(t) + k_i \int e(t)\, dt \tag{24}$$

After Laplace transformation, it becomes

$$U(s) = K_p E(S) + K_i \frac{E(S)}{s} \tag{25}$$

The equations can be shown in block diagram as shown in Figure 5. When the PI controller reaches the actuator limit, then the actuator becomes saturated. In this situation, the system effectively operates in open loop. To limit the integral windup, Figure 5 shows a significant anti-windup control scheme [16]. In the figure, three PI loops are used to control three interactive variables independently. The implementation is conventional and includes the term (*Kc.Excess*) to limit integral windup. *Excess* is calculated by subtracting the unlimited output (U) and limited output (*Out*). The term *Kc* multiplies the Excess and limits the accumulated integral portion (*Sum*). The pseudocode of the modified PI controller becomes:

Modified PI Controller pseudocode:
Error = *Ref* − *FB*
U = *Sum* + (*Kp***Error*)
If (*U* > *outMax*)
    Out = *outMax*
Else if (*U* < *outMin*)
    Out = *outMin*
Else
    Out = *U*
Excess = *U* − *Out*

Typical closed loop systems use PI controller through feedback mechanism to maintain the desired result. PI controllers can easily track DC quantities in low bandwidth condition. In the system, 3 phase AC quantities cannot be directly tracked by PI controller.

Thus, mathematical transformations such as Clarke and Park transformation provide an aid to convert the quantities into corresponding d-q components. Clarke Transformation converts three-phase AC signals as shown in Figure 6(a) into two-phase quadrature signals as shown in Figure 6(b). The equation for converting a, b, c frame into α, β frame is governed by the equation

$$\begin{bmatrix} f_\alpha(t) \\ f_\beta(t) \end{bmatrix} = \frac{2}{3}\begin{bmatrix} 1 & -\frac{1}{2} & -\frac{1}{2} \\ 0 & \frac{\sqrt{3}}{2} & -\frac{\sqrt{3}}{2} \end{bmatrix}\begin{bmatrix} f_a(t) \\ f_b(t) \\ f_c(t) \end{bmatrix} \tag{26}$$

For a balanced 3 phase system

$$f_a(t) + f_b(t) + f_c(t) = 0 \tag{27}$$

So, the Clarke transformation reduces into

$$f_\alpha(t) = \frac{2}{3} f_a(t) - \frac{1}{3}\left(f_b(t) + f_c(t)\right) \tag{28}$$

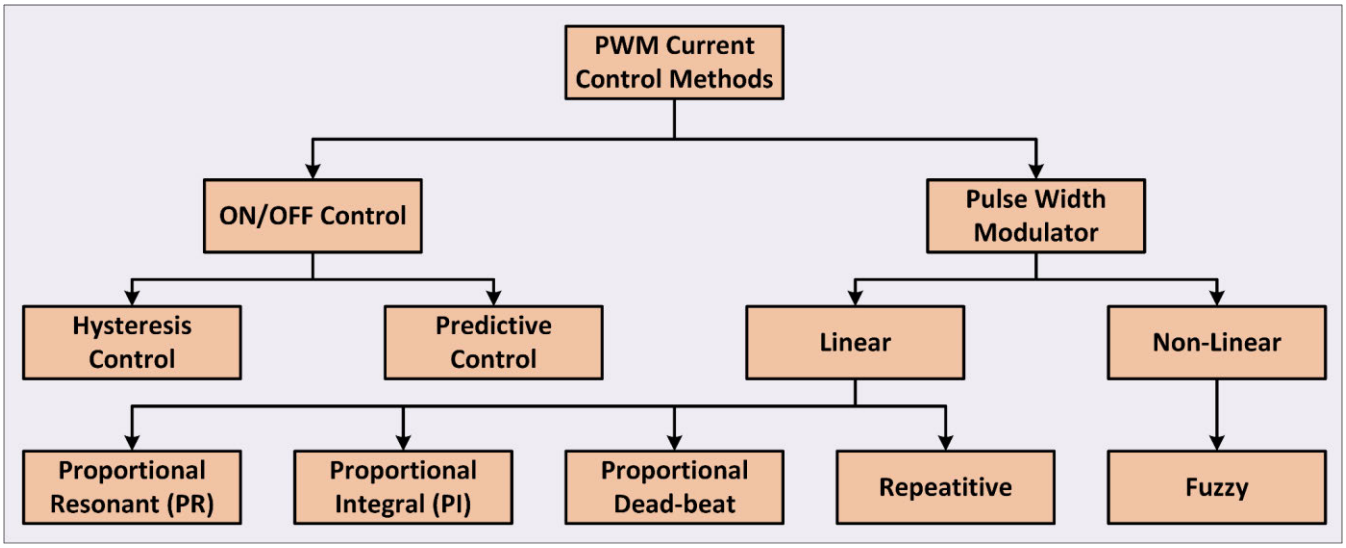

FIGURE 4. Classification of current control methods for VSI. The two primary types are on/off control (where switches are either on or off) and PWM control (where the pulse width of the signals can be controlled). From these two types emerge a vast classification of the current control methods.

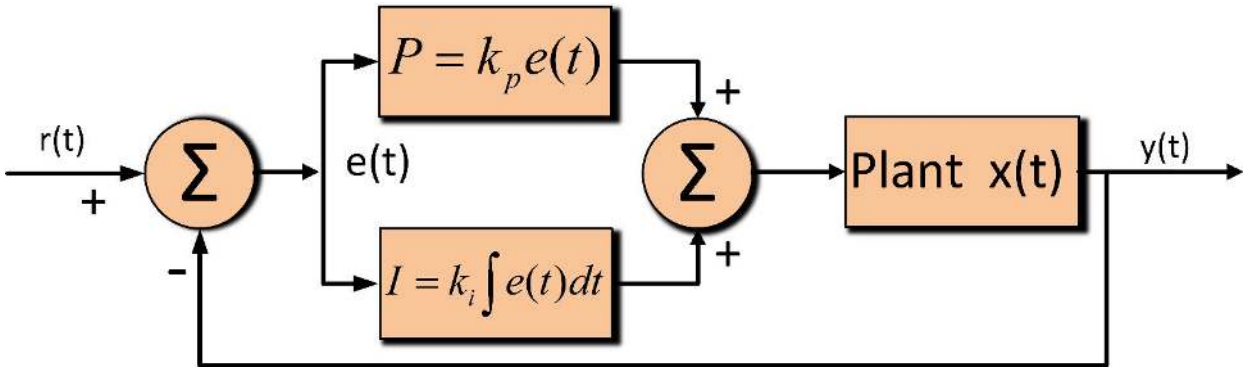

FIGURE 5. Block diagram of the closed loop system of the PI (proportional-integral) controller used in VSI along with associated equations. Here, k_p and k_i are the proportional and integral constants respectively, and e(t) is the error function of the input signal r(t); and y(t) is the output signal.

$$f_\alpha(t) = \frac{2}{3} f_a(t) - \frac{1}{3}(-f_a(t)) \tag{29}$$

$$f_\alpha(t) = f_a(t) \tag{30}$$

Similarly, $f_\beta(t)$ reduces into

$$f_\beta(t) = \frac{f_a(t) + 2f_b(t)}{\sqrt{3}} \tag{31}$$

The Park transformation results in DC quantities (d and q components) which can follow PI controller reference signal easily. The Park transformation of three-phase AC signals in Figure 6(a) results into the DC signals shown in Figure 6(c). The value of f_d and f_q can thus be derived from the predetermined value of $f_\alpha(t)$ and $f_\beta(t)$ using the following equation

$$\begin{bmatrix} f_d \\ f_q \end{bmatrix} = \begin{bmatrix} cos\theta(t) & sin\theta(t) \\ -sin\theta(t) & cos\theta(t) \end{bmatrix} \begin{bmatrix} f_\alpha(t) \\ f_\beta(t) \end{bmatrix} \tag{32}$$

The advantage of the reduced equations (30) and (31) is that it requires lesser number of multiplications than the equation (26). So, the transformation can be easily implemented into the dsPIC33F family microcontroller. These equations also dictate that only two phases (phase a and b) of voltage or current are needed to be sampled for the transformation.

IV. GRID SYNCHRONIZATION

The voltage amplitude and the frequency of the inverter and the grid need to be synchronized with each other when they are connected [17]. In the traditional synchronous generator system, the generator output voltage and frequency are the governing parameters to synchronize with the grid. After proper matching of amplitude and frequency, the generator synchronizes with the grid at the Point of Common Coupling (PCC). It needs to be continuously tracked on-line whether or not the synchronization is continually maintained. The condition of synchronization determines the firing signals for the inverter [18]. A grid tied inverter mimics the behavior of synchronous generators. So, to inject power into the grid,

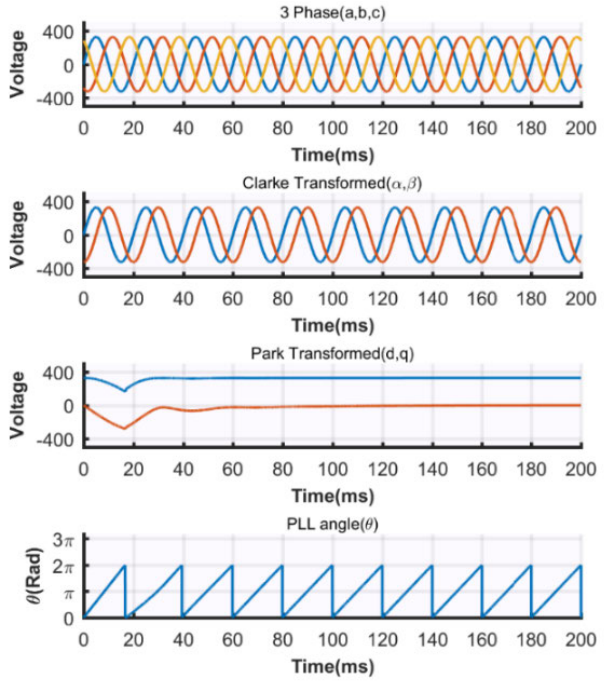

FIGURE 6. (a) Three-phase AC signals; (b) Clarke transformation of the AC signals; (c) Park transformation of the AC signals; (d) PLL angle of the AC signals.

it has to synchronize with the grid frequency and amplitude. There are several techniques for synchronization, such as [19]:

- Duplicate grid voltage output so that the output current reference has the same phase as the grid voltage
- Phase locked loop (PLL), a technique which samples grid voltage (Stationary frame PLL)
- Synchronous Reference Frame (d-q) PLL (SRF PLL)

SRF-PLL is used widely in ideal grid conditions for three-phase grid-connected power converters for its simple implementation and fast and accurate estimation of the phase/frequency [20]. Phase Locked Loop (PLL) is the heart of a grid tied inverter system, keeping track of the grid frequency and phase. More accurately, the role of PLL in a three-phase system is to estimate the angle measuring the instantaneous voltage waveform. The control of the grid tied inverter mainly depends on the synchronization algorithm. PLL synchronization techniques are prominently used in practical applications. A detailed discussion on PLL techniques can be found at [21]. Suppose, the PLL estimated angle is θ, then the a-b-c to d-q transformation can be described as

$$\begin{bmatrix} v_d \\ v_q \\ v_0 \end{bmatrix} = \sqrt{\frac{2}{3}} \begin{bmatrix} \cos(\theta) & \sin(\theta) & 0 \\ -\sin(\theta) & \cos(\theta) & 0 \\ 0 & 0 & 1 \end{bmatrix} \begin{bmatrix} \cos(\omega t) \\ \sin(\omega t) \\ 0 \end{bmatrix} \tag{33}$$

$$= \sqrt{\frac{2}{3}} \begin{bmatrix} \cos(\omega t)\cos(\theta) + \sin(\omega t)\sin(\theta) \\ -\sin(\theta)\cos(\omega t) + \cos(\theta)\sin(\omega t) \\ 0 \end{bmatrix} \tag{34}$$

Using trigonometric identity, the equation reduces to

$$\begin{bmatrix} v_d \\ v_q \\ v_0 \end{bmatrix} = \sqrt{\frac{2}{3}} \begin{bmatrix} \cos(\omega t - \theta) \\ \sin(\omega t - \theta) \\ 0 \end{bmatrix} \tag{35}$$

Under ideal grid conditions, the determined phase angle (θ) is equal to the phase angle of the grid (ωt) and as can be seen from the following equations; while v_q is equal to zero. The block diagram of the SRF-PLL system is illustrated in Figure 7. It is mandatory to assume that PLL is in locked mode during PLL design which means input signal and feedback signal are in phase and same frequency. When PLL angle is close to instantaneous voltage vector angle, $(\omega t - \theta)$ is small or close to zero. The term can be linearized for controlling using PI controller.

$$v_q = sin(\omega t - \theta) \approx (\omega t - \theta) \tag{36}$$

Thus, it can be concluded that, for balanced three-phase system, the q axis component V_q is close to zero when PLL angle is locked [22]. So, the q axis property is used in SRF-PLL as phase detector (PD) and low pass filter/PI controller is then used to eliminate steady state error and output is fed to voltage-controlled oscillator (VCO) which generates the angle and sine wave.

The transfer function of the PLL circuit is given by

$$H(s) = \frac{k_p s + \frac{k_p}{T_s}}{s^2 + k_p s + \frac{k_p}{T_s}} \tag{37}$$

We choose $T_s = 0.04$ and $\zeta = 1/\sqrt{2}$. So, the parameters of the PI controller can be calculated as

$$k_p = 2\zeta\omega_n = \frac{9.2}{T_s} \tag{38}$$

$$T_i = \frac{T_s \zeta^2}{2.3} \tag{39}$$

where, the natural frequency is given by

$$\omega_n = \frac{4.6}{\zeta T_s} \tag{40}$$

Figure 8 shows the three phase AC signals and the PLL angles for the signals.

All the necessary algorithms to implement grid tied inverters have been presented previously. This segment aims to present the PWM technique for generating output signal of inverter. There are many methods for generating PWM signals. In this application, Space Vector PWM (SVPWM) technique is implemented for its robustness [23].

The SVPWM subroutine can be implemented in three steps. In the first step, the sectors are calculated from the PLL angle. Secondly, the time durations t_0, t_1 *and* t_2 are to be calculated. After that, the duty cycle for different sectors can be easily determined according to the flowchart of Figure 9.

As shown in the figure, the first step to implement the SVPWM subroutine is to determine the sector from the PLL angle. That is done by comparing the extracted grid phase

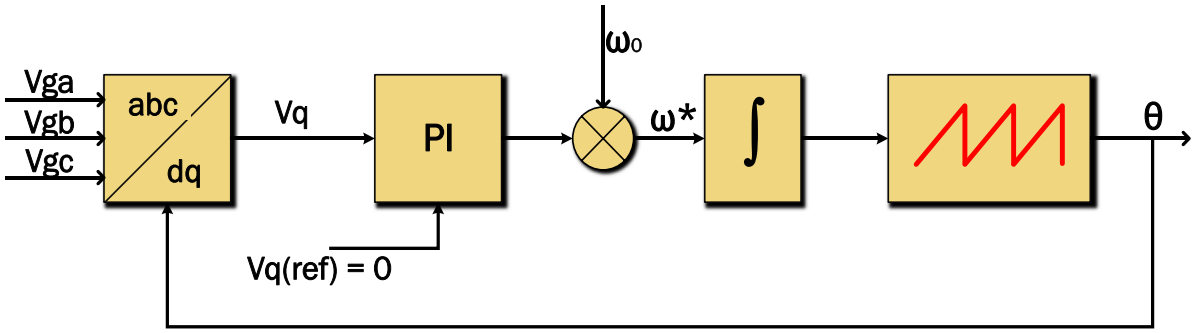

FIGURE 7. Block diagram of SRF-PLL for synchronizing the inverter to the grid. The three phases in abc frame are converted to the dq frame. Only the q axis component is used as phase detector for grid synchronization of the inverter.

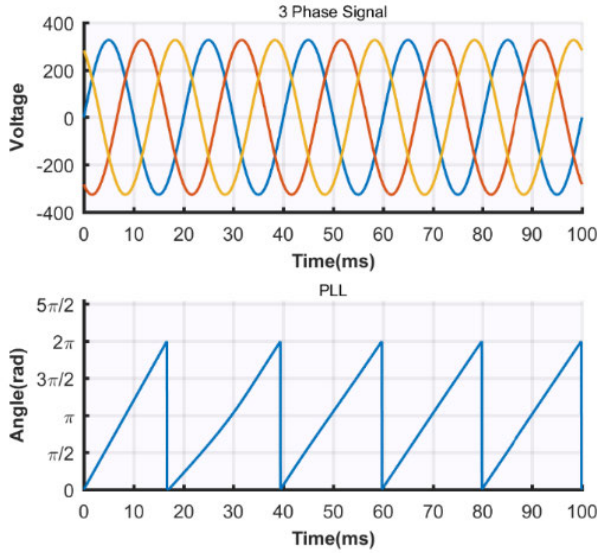

FIGURE 8. Simulation of the three-phase AC signals represented in red, blue and yellow (top) and the PLL angles (bottom).

TABLE 2. Duty cycles in sectors.

Sector	On Times of Inverter Upper Switch		
	Switch 1	Switch 2	Switch 3
1	$T_r + T_l + 0.5T_0$	$T_l + 0.5T_0$	$0.5T_0$
2	$T_r + 0.5T_0$	$T_r + T_l + 0.5T_0$	$0.5T_0$
3	$0.5T_0$	$T_r + T_l + 0.5T_0$	$T_l + 0.5T_0$
4	$0.5T_0$	$T_r + 0.5T_0$	$T_r + T_l + 0.5T_0$
5	$T_l + 0.5T_0$	$0.5T_0$	$T_r + T_l + 0.5T_0$
6	$T_r + T_l + 0.5T_0$	$0.5T_0$	$T_r + 0.5T_0$

angle with angle range of each sector, as illustrated in Figure 10. Table 2 demonstrates the duty cycles of the three upper switches of the inverter in the six different sectors.

The software implementation dsPIC controller is explained in the flowchart shown in Figure 11. The grid voltage and the current injected to the grid will be sensed firstly through ADC module of the dsPIC controller. Then the grid angle is extracted by the PLL algorithm. After that, the PI controller is executed for the current control loop. Finally, SVPWM subroutine is executed.

The second step to implement the SVPWM subroutine is to calculate the modulation index (m) and the time duration T_1, T_2, T_0 that can be determined by the following equations

$$m = \frac{u_{ref}}{u_{DC}/2} \tag{41}$$

$$T_1 = \frac{\sqrt{3}}{2} T_s m.sin\left(\frac{\pi}{3} - \theta\right) \tag{42}$$

$$T_2 = \frac{\sqrt{3}}{2} T_s m sin\,(\theta) \tag{43}$$

$$T_0 = T_s - T_1 - T_2 \tag{44}$$

where u_{ref} is the amplitude of desired output fundamental component, u_{DC} is the available dc-bus voltage, T_s is the sampling period, and s is the phase angle of the grid voltage that extracted by PLL.

The gating signals are generated when PWM module interrupts. The interrupt service routine for the PWM module is shown in Figure 12. In this routine, the duty cycle for each pair of PWM output (PWMxH/PWMxL) is loaded in its associated PWM duty cycle register (PDCx). After implementation of the SVPWM subroutine, the waveshapes of the three phases are represented in the simulation diagram shown in Figure 13.

V. MATHEMATICAL OPTIMIZATION

Fixed point math is an efficient method of calculating floating point number. In the computer processor perspective, all the calculations are performed in integer domain. Floating point-math takes many CPU cycles than fixed-point math whereas the floating point unit (FPU) is not present in the processor. Most of the 8-bit and 16-bit microcontrollers do not have FPU. In this application, the dsPIC33f family microchip microcontroller has been used, which is a 16-bit microcontroller with Digital Signal Processing (DSP) capabilities. Q1.15 is a popular fixed point format for 16-bit processor. Q1.15 represents 15 bits for fraction out of 16 bits. So, 16-bit signed value in integer math have a range of −32768 to +32767. In the Q1.15 math this range is represented as

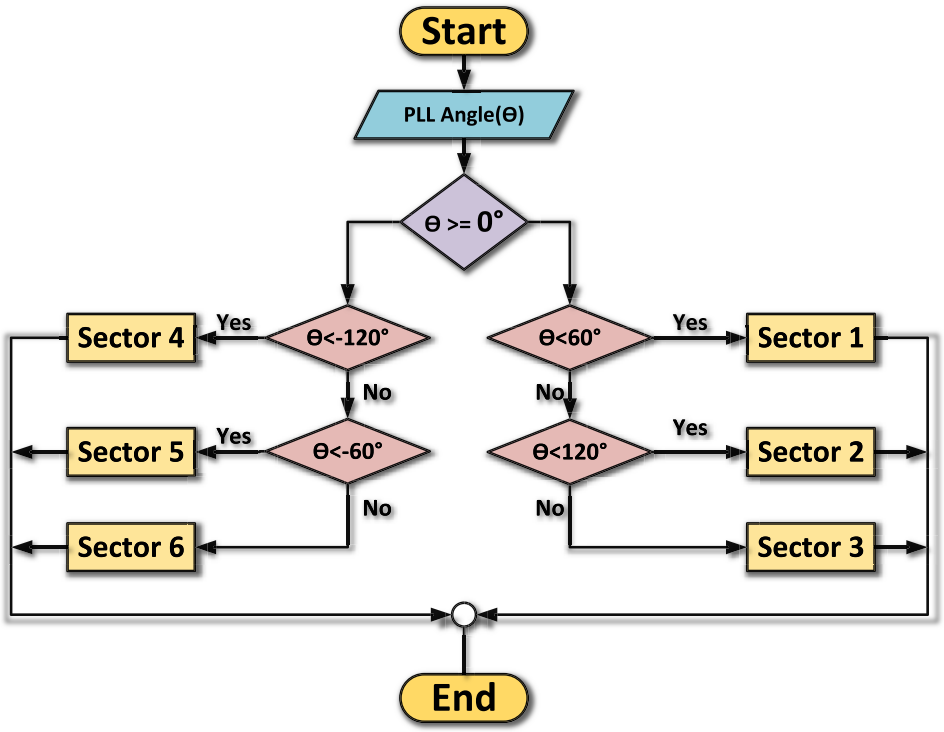

FIGURE 9. Flowchart depicting the steps for implementing the SVPWM subroutine. Firstly, the sectors are calculated from the reference signal from the controller. Then the modulation index and the time durations are calculated.

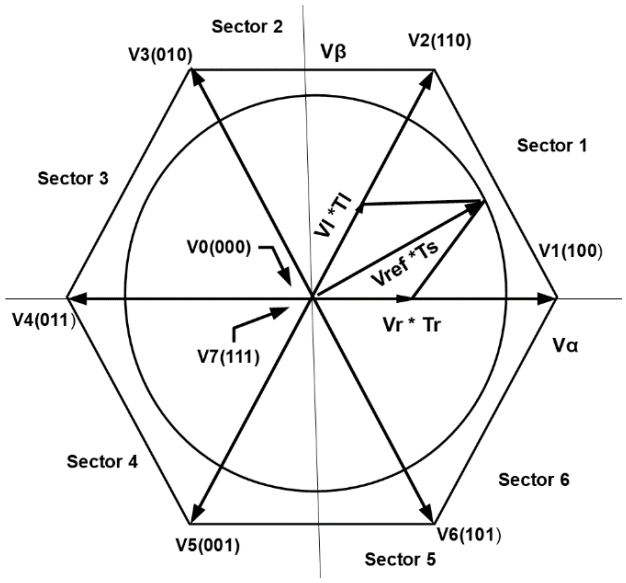

FIGURE 10. Determination of the sector of reference signal by comparing the extracted grid phase angle with the angle range of each sector.

−1.0 to+0.9999. There is another reason of using fixed point math instead of floating point math. That is, fixed-point math tends to saturate like real world behavior. For instance, the PLL angle varies from $+\pi$ to π in real world applications, whereas in Q1.15 format, this range represents −32768 to +32767.

TABLE 3. Some examples of fixed point implementation (in Q1.15 format) of floating point numbers.

Floating Point Operation	Q1.15 Equivalent
0.25+0.5 = 0.75	8192+16384 = 24576
0.5 x 0.5 = 0.25	16384 x 8192 = 24576
0.25/0.5 = 0.50	8192/16384 = 16384

$$Q15\,(x) = \begin{cases} 32768x - 0.5; & x < 0 \\ 32767x + 0.5; & x \geq 0 \end{cases} \tag{45}$$

Here, x represents any floating point value between −1 and 0.9999 and Q15(x) is fixed point representation of x in Q1.15 format. A few operations of how fixed point math performs floating point operations are demonstrated in Table 3. As all the calculations are in 16 bits. So, 32 bits output saturated into 16 bits.

VI. EXPERIMENTAL RESULTS

The proposed work is an assembly of several experimental steps. The successive development of the proposed model has been presented below through simulation diagrams. It is noteworthy that all the results obtained have been taken in fixed point arithmetic format and thereby, all the graphical results produced are scaled in the Q1.15 format along the vertical axis.

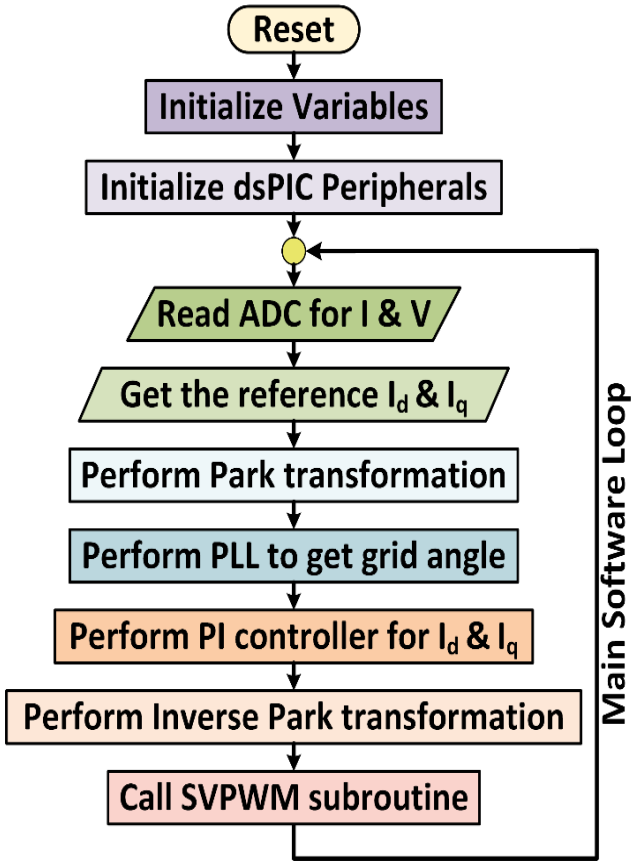

FIGURE 11. Flowchart illustrating the main routine for the dsPIC software prior to calling the SVPWM subroutine.

Here are the in short description of how we captured all the hardware results. We capture all the data using serial terminal. As serial terminal communication is low, so we used internal buffer for the variables. When buffer was full, data was sent through the serial terminal.

A. CLARKE TRANSFORMATION

The transformation from the abc-frame to the stationary $\alpha\beta$ frame is represented by Clarke transform, which is shown in Figure 14. Only two of the three phase voltages are fed into a Clarke transform to convert them from a three-phase system (i_a, i_b, i_c) to a two-dimensional orthogonal system (i_α, i_β). Note that it's not necessary to measure all three currents, since the sum of the three must equal unity (0). So, the third current must be the negative sum of the first two.

B. PARK TRANSFORMATION

The transformation from the stationary $\alpha\beta$ frame to the synchronously rotating dq frame is represented by Park transform, which is shown in Figure 15. A Park transform is used to convert the two-axis stationary system (i_α, i_β) to a two-axis rotating system (i_q, i_d). The main purpose to transform the three-phase instantaneous voltages and currents into the synchronously rotating reference dq frame is to make computations much easier. Besides, it allows the system operator to independently control the active (d-axis) and reactive (q-axis) components of the currents.

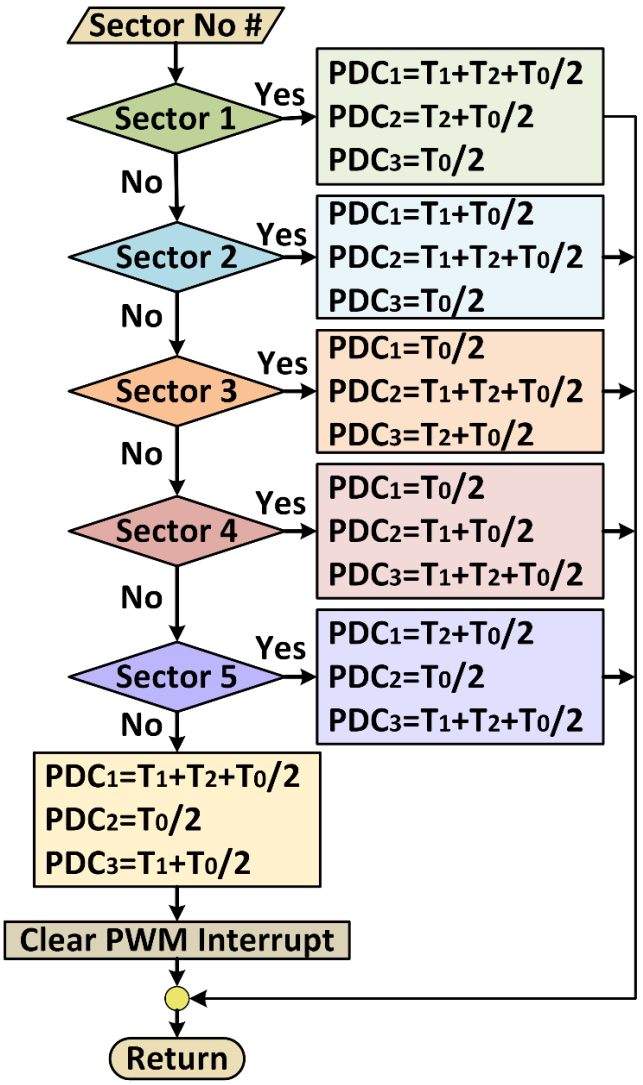

FIGURE 12. The interrupt service routine for PWM for generating the gating signals. Here, the duty cycle for each pair of PWM output (PWMxH/PWMxL) is loaded in its associated PWM duty cycle register (PDCx).

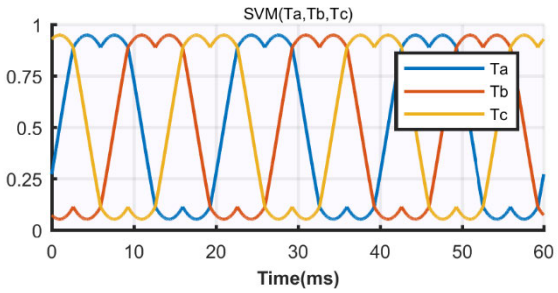

FIGURE 13. Output waveshapes of the three phases after implementation of the SVPWM subroutine, shown in red, blue and yellow. The waveshapes are not smooth sinusoidal.

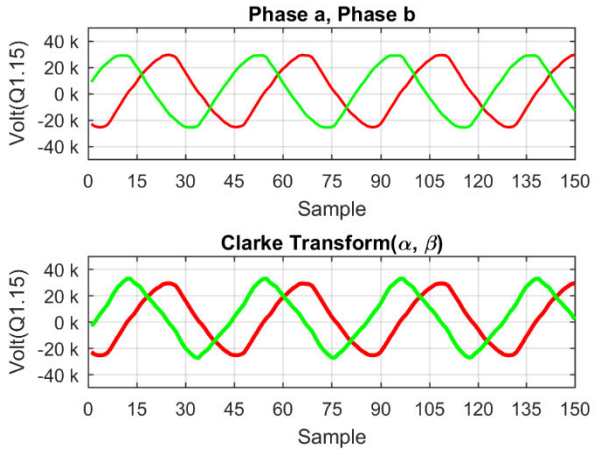

FIGURE 14. Demonstration of the Clarke Transformation: conversion of the axes system from three axis abc system to a two-axis stationary $\alpha\beta$ frame.

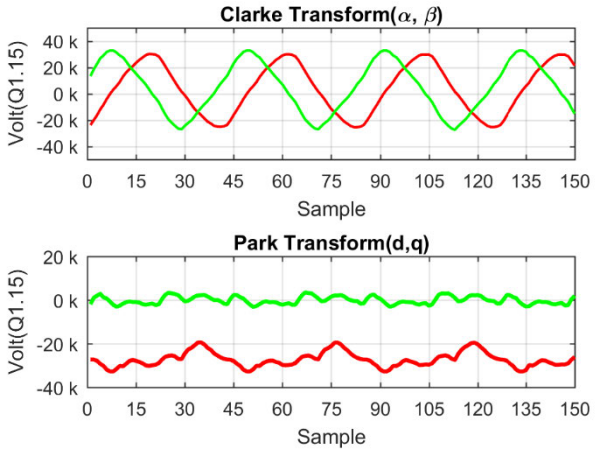

FIGURE 15. Demonstration of the Park Transformation; conversion of the axes system from the two axis stationary $\alpha\beta$ frame to the two axis rotating dq frame.

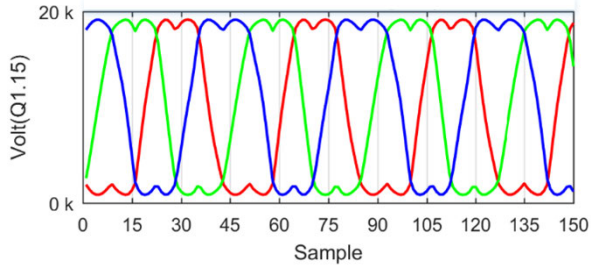

FIGURE 16. Simulation result of the implementation of the SVPWM subroutine. The three SVPWM phases are marked in red, blue and green.

C. SVPWM

SVPWM is employed in this system to generate appropriate gating pulses for the inverter. SVPWM has been proven to be a better technique compared to the more commonly used PWM or sinusoidal PWM (SPWM) techniques. SVPWM is generates a more fundamental sine wave with a higher voltage, dominant harmonic reduction and lower total harmonic distortion (THD) when used in an inverter. The three phases implementation of the SVPWM subroutine in dspic33f microcontroller is shown in Figure 16.

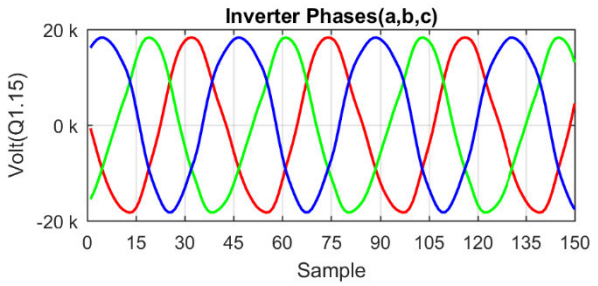

FIGURE 17. Demonstration of the simulated three output phase voltages of the inverter, shown in red, blue and green.

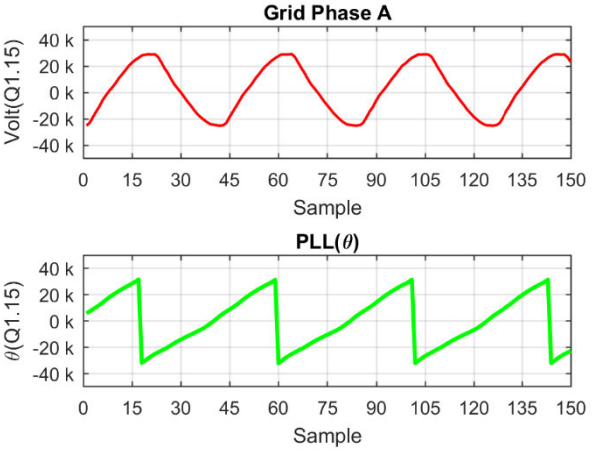

FIGURE 18. Simulation result of the PLL angles for one phase of the three-phase AC system. The other two phases show similar results.

D. INVERTER PHASES

The inverter takes input from the DC voltage source and converts it into three-phase AC voltage and feeds to the grid. For the experiment, a DC source is used instead of a solar array. The inverter converts the DC voltage into a three phase AC voltage. The three phases of the inverter output can be represented as the red, blue and green waveforms in Figure 17.

E. PLL

Phase locked loop (PLL) control is an indispensable part of the grid synchronization process. It helps to estimate the angular difference in the phase of the inverter output voltage and the grid voltage, based on which the VCO operates to control the frequency of the inverter output. Figure 18 represents the PLL angle of the inverter output voltage with respect to a certain phase of the grid.

F. PHASE SYNCHRONIZATION

Figure 19 shows the simulation of the grid synchronization process. The simulation has been illustrated for one phase only. The red waveform is the grid voltage and the green waveform is the inverter output voltage; and it is evident that these two waveforms are perfectly in phase with each other, i.e. with a phase difference of 0°. This implies that these two

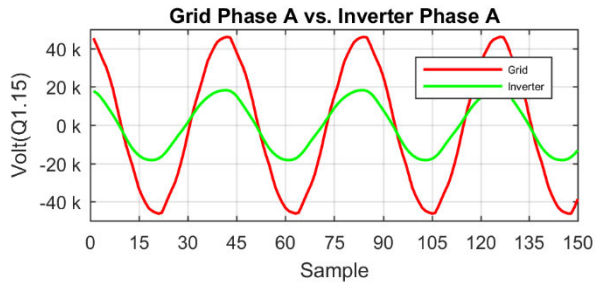

FIGURE 19. Simulation of the grid synchronization of one of the three phases of the AC voltage signal. The grid voltage and inverter voltage are in phase, implying that they are in synchronization.

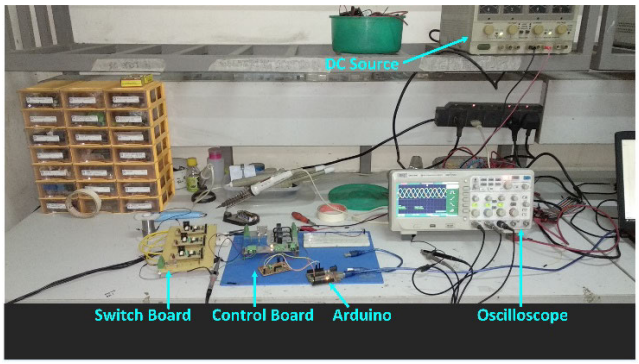

FIGURE 20. Components of the hardware implementation of the proposed three-phase grid tied inverter.

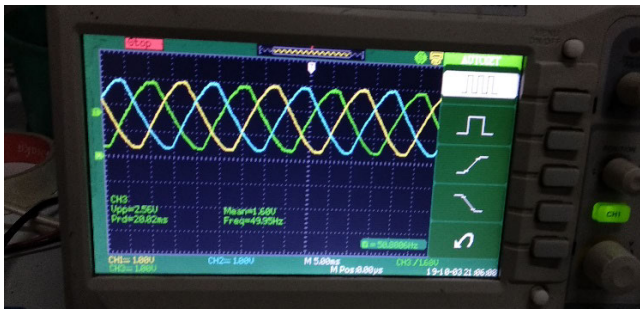

FIGURE 21. The three phases of the inverter output voltage as seen from the oscilloscope screen.

signals are matched in phase and therefore, the inverter output has been synchronized with the grid voltage.

G. HARDWARE IMPLEMENTATION

The components used in the hardware implementation of the proposed model has been presented as an image in Figure 20. The three-phase 400V, 50Hz AC signal output voltage of the inverter, which is fed to the grid, is sampled by a sensor board, which can be observed on the oscilloscope display, as shown in Figure 21. There is a control board and a switch board too. A serial converter aids to display the waveforms on the monitor. The monitor depicts the live control of the device, as shown in Figure 22. The monitor shows four waveforms: the PLL angles, and the three SVM phases, which are similar

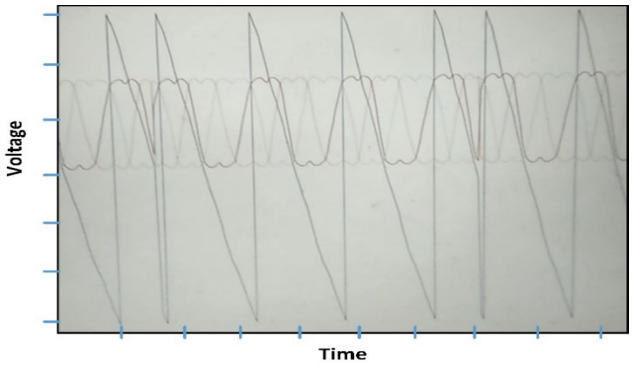

FIGURE 22. The simulation of the PLL angle (triangular) and the three SVM phases (three colors) as seen from the monitor screen.

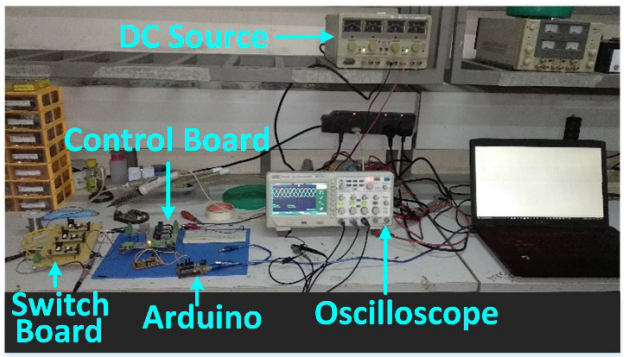

FIGURE 23. Image of the complete hardware implementation of the proposed system of the grid tied three-phase inverter.

to Figure 8 (bottom) and Figure 14. The complete hardware implementation setup is shown in the image of Figure 23. In the hardware implementation, a DC source is directly used instead of a PV system for the purpose of experimentation and convenience.

VII. CONCLUSION

In this paper, a grid tied inverter has been proposed which can be implemented using fixed point calculation and digital signal processing (DSP). The fixed point arithmetic and DSP implementation have been found to perform better than the conventional methods of calculation, yielding a low-cost inverter. A hardware model of such a grid tied inverter has also been implemented in this work. The current control strategy has been used for the voltage source inverter in the proposed system. PI controller has been used for the current control strategy. Space Vector Pulse Width Modulation (SVPWM) technique has been used for generating the gating pulses. For the purpose of grid synchronization, Synchronous Reference Frame Phase Locked Loop (SRF-PLL) has been employed. MATLAB/Simulink platform has been used for simulations and to assess the feasibility of the hardware model. Future works will include improvisation of the proposed system to make it more cost-effective and tolerant of intermittencies of renewable sources of energy by incorporating an energy storage system along with this system.

REFERENCES

[1] H. Keyhani, M. Johnson, and H. A. Toliyat, "A soft-switched highly reliable grid-tied inverter for PV applications," in *Proc. IEEE Appl. Power Electron. Conf. Exposit. (APEC)*, Fort Worth, TX, USA, Mar. 2014, pp. 1725–1732.

[2] Q. Zhao, Y. Ye, G. Xu, C. He, M. Zhu, D. Wang, and T. Liu, "Improved cascade-type repetitive control of grid-tied inverter with LCL filter," in *Proc. 13th Int. Conf. Control Autom. Robot. Vis. (ICARCV)*, Singapore, Dec. 2014, pp. 1439–1443.

[3] Y. Zhou and H. Li, "Analysis and suppression of leakage current in cascaded-multilevel-inverter-based PV systems," *IEEE Trans. Power Electron.*, vol. 29, no. 10, pp. 5265–5277, Oct. 2014.

[4] W. Wu, S. Feng, J. Ji, M. Huang, and F. Blaabjerg, "LLCL-filter based single-phase grid-tied aalborg inverter," in *Proc. Int. Power Electron. Appl. Conf. Exposit.*, Shanghai, China, Nov. 2014, pp. 658–663.

[5] H. Nunes, N. Pimenta, L. Fernandes, P. Chaves, and J. D. Costa, "Modular buck-boost transformerless grid-tied inverter for low voltage solar panels," in *Proc. Int. Conf. Renew. Energies Power Qual.*, 2014, pp. 109–114.

[6] S. Shuvo, E. Hossain, T. Islam, A. Akib, S. Padmanaban, and M. Z. R. Khan, "Design and hardware implementation considerations of modified multilevel cascaded H-bridge inverter for photovoltaic system," *IEEE Access*, vol. 7, pp. 16504–16524, 2019.

[7] M. H. Mondol, M. R. Tur, S. P. Biswas, M. K. Hosain, S. Shuvo, and E. Hossain, "Compact three phase multilevel inverter for low and medium power photovoltaic systems," *IEEE Access*, vol. 8, pp. 60824–60837, 2020.

[8] A. Abdalrahman, A. Zekry, and A. Alshazly, "Simulation and implementation of grid-connected inverters," *Int. J. Comput. Appl.*, vol. 60, no. 4, pp. 41–49, Dec. 2012.

[9] A. Al-Durra, A. Reznik, M. G. Simoes, and S. M. Muyeen, "Performance analysis of a grid-tied inverter for renewable energy applications," in *Proc. 40th Annu. Conf. IEEE Ind. Electron. Soc. (IECON)*, Dallas, TX, USA, Oct. 2014, pp. 4981–4987.

[10] F. Sevilmis and H. Karaca, "An experimental study of grid tied inverter for renewable energy systems," in *Proc. Int. Conf. Smart Energy Syst. Technol. (SEST)*, Sep. 2018, pp. 1–6, doi: 10.1109/SEST.2018.8495826.

[11] T. Hornik and Q.-C. Zhong, "A current-control strategy for voltage-source inverters in microgrids based on H^{∞} and repetitive control," *IEEE Trans. Power Electron.*, vol. 26, no. 3, pp. 943–952, Mar. 2011.

[12] Q. Zeng and L. Chang, "Study of advanced current control strategies for three-phase grid-connected PWM inverters for distributed generation," in *Proc. IEEE Conf. Control Appl. (CCA)*, Toronto, ON, Canada, Aug. 2005, pp. 1311–1316.

[13] M. P. Kazmierkowski and L. Malesani, "Current control techniques for three-phase voltage-source PWM converters: A survey," *IEEE Trans. Ind. Electron.*, vol. 45, no. 5, pp. 691–703, Oct. 1998.

[14] A. Abdalrahman and A. Zekry, "Control of the grid-connected inverter using dsPIC microcontroller," in *Proc. 2nd Int. Japan-Egypt Conf. Electron., Commun. Comput. (JEC-ECC)*, Dec. 2013, pp. 159–164.

[15] S. Eren, A. Bakhshai, and P. Jain, "Control of three-phase voltage source inverter for renewable energy applications," in *Proc. IEEE 33rd Int. Telecommun. Energy Conf. (INTELEC)*, Amsterdam, The Netherlands, Oct. 2011, pp. 1–4.

[16] Y. Sozer and D. A. Torrey, "Modeling and control of utility interactive inverters," *IEEE Trans. Power Electron.*, vol. 24, no. 11, pp. 2475–2483, Nov. 2009.

[17] *Sensorless Field Oriented Control (FOC) of a Permanent Magnet Synchronous Motor (PMSM)*, Microchip Technol. Inc., Chandler, AZ, USA, 2010.

[18] K. Arulkumar, K. Palanisamy, and D. Vijayakumar, "Recent advances and control techniques in grid connected Pv system—A review," *Int. J. Renew. Energy Res.*, vol. 6, pp. 1037–1049, Jun. 2016.

[19] F. D. Freijedo, J. Doval-Gandoy, Ó. López, C. Martinez-Peñalver, A. G. Yepes, P. Fernandez-Comesana, J. Malvar, A. R. Nogueiras, J. Marcos, and A. Lago, "Grid-synchronization methods for power converters," in *Proc. 35th Annu. Conf. IEEE Ind. Electron.*, Nov. 2009, pp. 522–529.

[20] X. Zong, *A Single Phase Grid Connected DC/AC Inverter With Reactive Power Control for Residential PV Application*. Toronto, ON, Canada: Univ. of Toronto, 2011.

[21] N. Jaalam, N. A. Rahim, A. H. A. Bakar, C. Tan, and A. M. A. Haidar, "A comprehensive review of synchronization methods for grid-connected converters of renewable energy source," *Renew. Sustain. Energy Rev.*, vol. 59, pp. 1471–1481, Jun. 2016, doi: 10.1016/j.rser.2016.01.066.

[22] Z. Ali, N. Christofides, L. Hadjidemetriou, E. Kyriakides, Y. Yang, and F. Blaabjerg, "Three-phase phase-locked loop synchronization algorithms for grid-connected renewable energy systems: A review," *Renew. Sustain. Energy Rev.*, vol. 90, pp. 434–452, Jul. 2018.

[23] M. Bhardwaj, "Software phase locked loop design using C2000 microcontrollers for single phase grid connected inverter," Texas Instrum., Dallas, TX, USA, Appl. Rep. SPRABT3A, 2013.

[24] Z. R. Rony, S. C. Das, and M. Z. Rahman Khan, "Space vector modulated PWM generation for motor control systems," in *Proc. 10th Int. Conf. Electr. Comput. Eng. (ICECE)*, Dec. 2018, pp. 149–152, doi: 10.1109/ICECE.2018.8636720.

SHUVANGKAR SHUVO (Member, IEEE) received the B.Sc. degree in electrical and electronic engineering from the Bangladesh University of Engineering and Technology (BUET), in 2017. He is currently working on power electronics, smart grid/microgrid, and energy storage systems.

EKLAS HOSSAIN (Senior Member, IEEE) received the B.S. degree in electrical and electronic engineering from the Khulna University of Engineering and Technology, Bangladesh, in 2006, the M.S. degree in mechatronics and robotics engineering from the International Islamic University of Malaysia, Malaysia, in 2010, and the Ph.D. degree from the College of Engineering and Applied Science, University of Wisconsin Milwaukee (UWM). He was worked in the area of distributed power systems and renewable energy integration for last ten years. He has been involved with several research projects on renewable energy and grid tied microgrid system with Oregon Tech, as an Assistant Professor with the Department of Electrical Engineering and Renewable Energy, since 2015. He is currently working as an Associate Researcher with the Oregon Renewable Energy Center (OREC). He is also a registered Professional Engineer (PE) with the state of Oregon, USA. He is also a Certified Energy Manager (CEM) and a Renewable Energy Professional (REP). He has published a number of research articles and posters in this field. His research interests include modeling, analysis, design, and control of power electronic devices, energy storage systems, renewable energy sources, integration of distributed generation systems, microgrid and smart grid applications, robotics, and advanced control systems. He is a Senior Member of Association of Energy Engineers (AEE). He is the winner of the Rising Faculty Scholar Award in 2019 from the Oregon Institute of Technology for his outstanding contribution in teaching. He is also serving as an Associate Editor of IEEE Access. He, with his dedicated research team, is looking forward to explore methods to make the electric power systems more sustainable, cost-effective and secure through extensive research and analysis on energy storage, microgrid systems, and renewable energy sources.

ZIAUR RAHMAN KHAN is currently working with the Department of Electrical and Electronic Engineering, Bangladesh University of Engineering and Technology. He conducts research in power electronics, renewable energy systems, electronic device modeling and simulation engineering, and electrical engineering.